Hindawi
Journal of Spectroscopy
Volume 2018, Article ID 3413864, 8 pages
https://doi.org/10.1155/2018/3413864

Research Article

Orange-Reddish Light Emitting Phosphor $GdVO_4:Sm^{3+}$ Prepared by Solution Combustion Synthesis

M. S. Rabasovic,[1] **J. Krizan**,[2] **S. Savic-Sevic**,[1] **M. Mitric**,[3] **M. D. Rabasovic**,[1] **B. P. Marinkovic**,[1] **and D. Sevic**[1]

[1]*Institute of Physics, University of Belgrade, P.O. Box 68, Pregrevica 118, 11080 Belgrade, Serbia*
[2]*AMI d.o.o, Ptuj, Slovenia*
[3]*Vinca Institute of Nuclear Science, University of Belgrade, P.O. Box 522, 11001 Belgrade, Serbia*

Correspondence should be addressed to D. Sevic; sevic@ipb.ac.rs

Received 12 December 2017; Accepted 16 April 2018; Published 2 May 2018

Academic Editor: Damien Boyer

The gadolinium vanadate doped with samarium ($GdVO_4:Sm^{3+}$) nanopowder was prepared by the solution combustion synthesis (SCS) method. After synthesis, in order to achieve the full crystallinity, the material was annealed in air atmosphere at 900°C. Phase identification in the postannealed powder samples was performed by X-ray diffraction, and morphology was investigated by high-resolution scanning electron microscopy (SEM). Photoluminescence characterization of the emission spectrum and time-resolved analysis have been performed using the tunable laser optical parametric oscillator excitation and the streak camera. Several strong emission bands in the Sm^{3+} emission spectrum were observed, located at 567 nm ($^4G_{5/2}$–$^6H_{5/2}$), 604 nm ($^4G_{5/2}$–$^6H_{7/2}$), and 646 (654) nm ($^4G_{5/2}$–$^6H_{9/2}$), respectively. The weak emission bands at 533 nm ($^4F_{3/2}$–$^6H_{5/2}$) and 706 nm ($^4G_{5/2}$–$^6H_{11/2}$) and a weak broad luminescence emission band of VO_4^{3-} were also observed by the detection system. We analyzed the possibility of using the host luminescence for two-color temperature sensing. The proposed method is improved by introducing the temporal dependence in the line intensity ratio measurements.

1. Introduction

Many investigations have been devoted to rare earth orthovanadates RVO_4 (R = Sc, Y, La, Gd, or Lu) (see [1–4] and references therein). Gadolinium vanadate ($GdVO_4$) is a very important host for the luminescence of rare earth activators which find applications in the high-power solid state lasers, X-ray medical radiography, energy-saving fluorescent lamps, artificial production of light, other display devices [5–11], and temperature sensing [4]. Phosphors based on gadolinium compounds play an important role because the Gd^{3+} ion ($4f^7$) has its lowest excited level at relatively high energy, which is due to the stability of the half-filled shell ground state [6]. The $GdVO_4$:Sm nanopowder is an efficient orange-reddish light emitting material due to a strong absorption of ultraviolet light by $GdVO_4$ and efficient energy transfer from vanadate groups (VO_4^{3-}) to dopants (Sm^{3+}).

In this paper, we present the results of experimental investigation of Sm^{3+}-doped $GdVO_4$ nanopowders, prepared by the solution combustion synthesis (SCS) method [12, 13].

Simplicity and low cost are the main characteristics of this process. Phase identification in the postannealed powder samples was performed by X-ray diffraction, and morphology was investigated by high-resolution scanning electron microscopy (SEM). The main aim of this study is time-resolved analysis of luminescence properties of $GdVO_4:Sm^{3+}$ nanopowders. The possibility for $GdVO_4:Sm^{3+}$ usage in phosphor thermometry was analyzed in [4], where temperature determination of sensing calibration curves was based on intensity ratios of luminescence of samarium lines. Here, we have taken a different approach. First, we use intensity

ratio of the host and samarium line luminescence emissions (two-color thermometry). This new approach to the ratiometric luminescence thermometry was proposed recently, using TiO_2 nanopowders doped with Eu^{3+} [14] and Sm^{3+} [15], Zn_2SiO_4 doped with Mn^{2+} [16], and Eu^{3+} $Gd_2Ti_2O_7$ doped with Eu^{3+} [17]. So, this concept, used in our study, provides high relative sensitivities by itself. However, the method presented here is further improved by introducing the temporal dependence in the luminescence intensity ratio measurements, as proposed in [18], providing even more increased sensitivity.

2. Experimental

2.1. Synthesis. $GdVO_4$ nanopowder doped with samarium ions was prepared by the solution combustion method, as described in [12, 13]. Stoichiometric quantities of starting chemicals $Sm(NO_3)_3$, $Gd(NO_3)_3 * 6H_2O$, and NH_4VO_3 with the purity of 99.99% were chosen to obtain the Sm^{3+} concentration in $GdVO_4$ of 1 at.% ($Gd_{1-0.01}Sm_{0.01}VO_4$). The used chemicals and ammonium nitrate (NH_4NO_3) were purchased from ABCR, and urea ($(NH_2)_2CO$) from Sigma-Aldrich. The dry mixture of 0.134 g (0.4 mmol) of $Sm(NO_3)_3$, 18.05 g (40 mmol) of $Gd(NO_3)_3*6H_2O$, and 4.676 g (40 mmol) of NH_4VO_3 was combined with the mixture of 4.8 g (60 mmol) of ammonium nitrate and 3.003 g (50 mmol) of urea which were used as organic fuels. The prepared starting reagents were combusted with the flame burner at approximately 500°C, yielding a voluminous foamy powder in an intensive exothermic reaction. After the solution combustion synthesis, the nanopowder was annealed for 2 hours, in air atmosphere, at 900°C. Annealing has an effect on increasing the grain size of the nanopowders, and it is widely used to achieve the higher emission intensity.

2.2. Instruments and Measurements. The structure of the nanopowder was verified by X-ray diffraction analysis, using a Philips PW 1050 instrument, with Ni filtered $Cu \cdot K_{\alpha 1,2}$ radiation ($\lambda = 0.15405$ nm). X-ray diffraction measurements were done at room temperature over the 2θ range of 10–90° with a scanning step width of 0.05° and a counting time of 8 s per step. The morphology of nanopowders and the size of crystallites were determined by high-resolution scanning electron microscopy (SEM) equipped with a high-brightness Schottky field emission gun (FEGSEM, TESCAN) operating at 4 kV. Photoluminescence (PL) studies reported in this work were performed using an optical parametric oscillator (Vibrant OPO), as described in [12, 13]. The output of the OPO can be continuously tuned over a spectral range from 320 nm to 475 nm. Time-resolved streak images of the emission spectrum excited by the OPO system were collected by using a spectrograph (SpectraPro 2300i) and recorded with a Hamamatsu streak camera (model C4334). All streak camera operations were controlled by the HPD-TA (High Performance Digital Temporal Analyzer) software. We used a homemade temperature control system for luminescence measurements presented here.

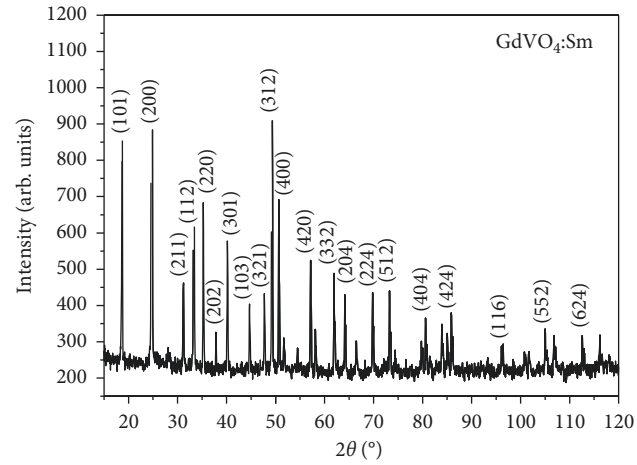

FIGURE 1: The XRD patterns of the $GdVO_4$:Sm nanopowder with respective Miller indices.

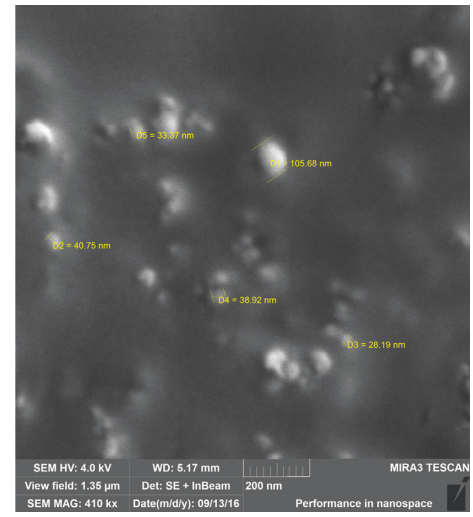

FIGURE 2: The SEM image of the $GdVO_4$:Sm nanopowder annealed at 900°C.

3. Results

3.1. XRD and SEM Study. In order to know the structural properties and differences in the phase purities of the prepared $GdVO_4$:Sm nanopowder, XRD analysis was recorded and is presented in Figure 1. XRD confirmed the successful formation of the pure-phase $GdVO_4$ powder with the $I4_1/amd$ space group (JCPDS Card no. 86-0996). Ionic radius of the Sm^{3+} ion (0.964 Å) is a slightly larger than that of Gd^{3+} ion (0.938 Å), which indicates that Sm^{3+} could be successfully incorporated into the $GdVO_4$ host lattice by substituting Gd^{3+} without changing the tetragonal zircon type structure of $GdVO_4$ [9]. The particle size and morphology of the $GdVO_4$:Sm nanopowder annealed at 900°C were characterized by SEM (Figure 2). Some particles are agglomerated as clusters; however, individual spherical-shaped particles are also visible and labeled in Figure 2. The average grain size, D, was estimated by the Scherer equation, $D = K\lambda/\beta \cos\theta$, where K is a constant related to

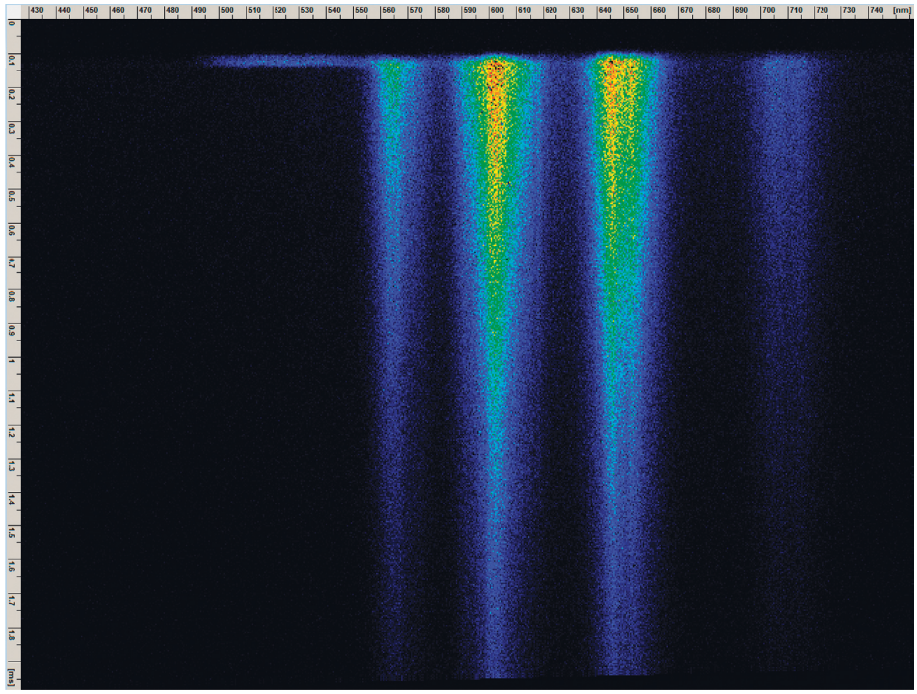

Figure 3: The streak image of the photoluminescence spectrum of $GdVO_4:Sm^{3+}$ nanophosphor (OPO excitation at 330 nm).

the shape of the crystallite and is approximately equal to unity, we used $K = 0.89$ as in [19], λ is the X-ray wavelength (0.15405 nm), and θ and β are the diffraction angle and full width at half maximum (FWHM, in radians) of the corresponding peak, respectively. The strongest peaks (2θ) from XRD were used to calculate the average crystallite size (D) in the $GdVO_4$:Sm nanopowder. The estimated particle size is about 43 nm. The SEM image (Figure 2) reveals that sizes of individual particles of nanopowders are between 30 nm and 105 nm, which is in agreement with the calculated averaged result from XRD.

3.2. Photoluminescence and Lifetime Analysis. The streak image of the time-resolved photoluminescence spectrum of the $GdVO_4:Sm^{3+}$ nanopowder using the 330 nm excitation is presented in Figure 3. Horizontal scale of the streak image corresponds to wavelength, and the vertical scale shows development of spectra in time. Images are presented in pseudocolor, where different colors mean different optical intensities.

Spectral characteristics of luminescence emission intensities of the synthesized $GdVO_4:Sm^{3+}$ (1 at.%) nanopowder sample are shown in Figure 4. The spectrum was obtained by integrating in time the spectral image acquired by the streak camera in the photon counting mode, with the time scale of 5 ms, at the excitation of 330 nm.

It could be seen in Figure 4 that the $GdVO_4$:Sm nanopowder sample have comparable luminescence emission intensities in green, orange, and red regions. All those emission bands correspond to the transitions from excited energy level $^4G_{5/2}$ of Sm^{3+} ion to $^6H_{5/2}$ (~567 nm), $^6H_{7/2}$ (602 nm), $^6H_{9/2}$ (646 and 654 nm), and $^6H_{11/2}$ (~706 nm) level, respectively. The strong emission of Sm^{3+} is due to efficient energy transfer from the VO_4^{3-} group to Sm^{3+} ion

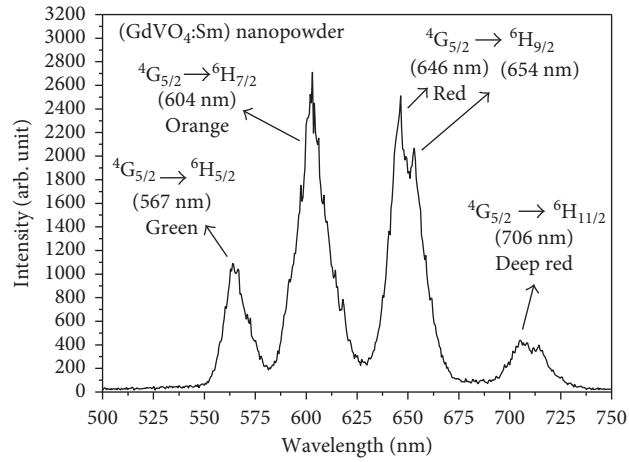

Figure 4: The photoluminescence (PL) emission spectrum of our $GdVO_4$:Sm nanopowder sample (OPO excitation at 330 nm).

in the $GdVO_4:Sm^{3+}$ sample. However, the deep red emission of these samples is almost on the end of the region of human eye color sensitivity, so the small influence of this emission on the color chromaticity coordinates of $GdVO_4:Sm^{3+}$ is expected. The transitions at 604 and 646 nm have relatively higher emission intensities over the other transitions causing an orange-reddish emission from the Sm^{3+}.

Fluorescence lifetime analysis for the $GdVO_4:Sm^{3+}$ nanopowder has also been performed, and the obtained result is presented in Figure 5. We present the fluorescence lifetime analysis for the most intense emission peak ($^4G_{5/2}$–$^6H_{7/2}$) in Sm^{3+} ion. Luminescence decay curve is well fitted using a double-exponential function. The average luminescence lifetime can be determined by the following formula [20–24]:

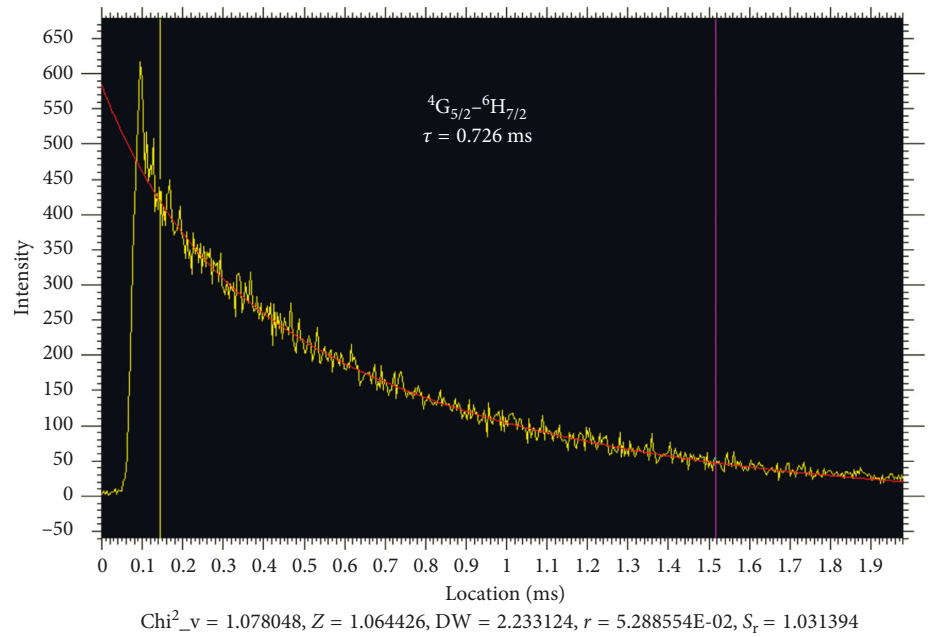

Figure 5: The luminescence decay curve for the $^4G_{5/2}$–$^6H_{7/2}$ transition in Sm^{3+} ion fitted by a double-exponential decay.

$$\tau = \frac{\left(A_1\tau_1^2 + A_2\tau_2^2\right)}{\left(A_1\tau_1 + A_2\tau_2\right)}, \quad (1)$$

where A_1 and A_2 denote the amplitudes of respective decay components and τ_1 and τ_2 are fluorescence lifetime components contributing to the average lifetime. The obtained result for average lifetime for Sm^{3+} ion is 0.726 ms. It is found that our result for lifetime of Sm^{3+} ion in the $GdVO_4$ nanopowder is longer in comparison with 0.66 ms [20], 0.55 ms [25], and 0.42 ms [6]. It is well known that the luminescent lifetime of rare earth ion is influenced by the structure of the host, the rare earth located sites (on the surface or bulk) of the host, defects, and impurity [26]. The defect and impurity may act as quenching centers and reduce luminescent lifetime.

The double-exponential decay behavior of the activator is frequently observed when the excitation energy is transferred from the donor [6]. The energy transfer is not the main cause of the deviation from the single-exponential behavior of the decay curve since the energy transfer from the VO_4^{3-} groups to Sm^{3+} ions mainly influences the rise time of the decay curve [27]. The streak image of $GdVO_4$:Sm^{3+} nanopowder luminescence with a time scale of 100 μs is shown in Figure 6. In this time scale, the host luminescence and weak samarium line at 533 nm ($^4F_{3/2}$–$^6H_{5/2}$), barely discernible and not denoted in Figures 3 and 4, are easily identified. In our measurements, all luminescence bellow 500 nm is cut off by the optical filter used for blocking the OPO excitation. The spectral shape of host luminescence, detected by us only above 500 nm, is similar to spectra presented in [1, 9, 28]. The $GdVO_4$ luminescence is ascribed to the VO_4^{3-} group. Calculated lifetime of host luminescence of 2.82 μs agrees well with the time-resolved analysis provided in [28]. Moreover, as we have shown in the next subsection, this luminescence is gradually quenched by raising the temperature, which means that it is not measuring error caused by stray light of laser excitation.

The estimated rise time of samarium luminescence shown in Figure 6 is negligible for effects of interest. For used time scale, it is determined mainly by the instrumental response. So, the multiexponential behavior should be ascribed to the absorbed impurities, which lead to the defects and the quenching centers [27, 29]. Decay kinetics behavior depends also on the number of different luminescent centers [20, 27]. If rare earth ions occupy several different sites in host lattices, they can generate several different luminescent centers which lead to a multiexponential behavior [29]. Tian et al. [30] explained that, in Dy^{3+}-doped bulk $GdVO_4$:Dy phosphors, the energy transfers mainly happen between Dy^{3+} ions [31, 32]. In the case of nanoparticles, the energy transfer starting from the luminescent level can be more complicated, since the defects, which can act as quenching centers, in nanoparticles are more plenteous than those in bulk phosphors [29, 31, 33]. Due to the defects produced during the preparation process and trace impurities contained in the raw materials, the samples necessarily have quenching centers (traps) with very low concentrations. When the excited luminescent center is in the vicinity of the trap, the excited energy could be transferred easily to the trap from which it is lost nonradiatively [33]. As a result, decay time should become short. In our case, longer lifetime of 0.726 ms may be due to the better crystallization and less defects, which reduces the nonradiative probability and results in the longer lifetimes.

3.3. Temperature Sensing Using $GdVO_4$:Sm Nanophosphor. Recently, the new concept of using the host luminescence for the fluorescence intensity ratio method was introduced (see [14–17] and references therein). In our study, the method is

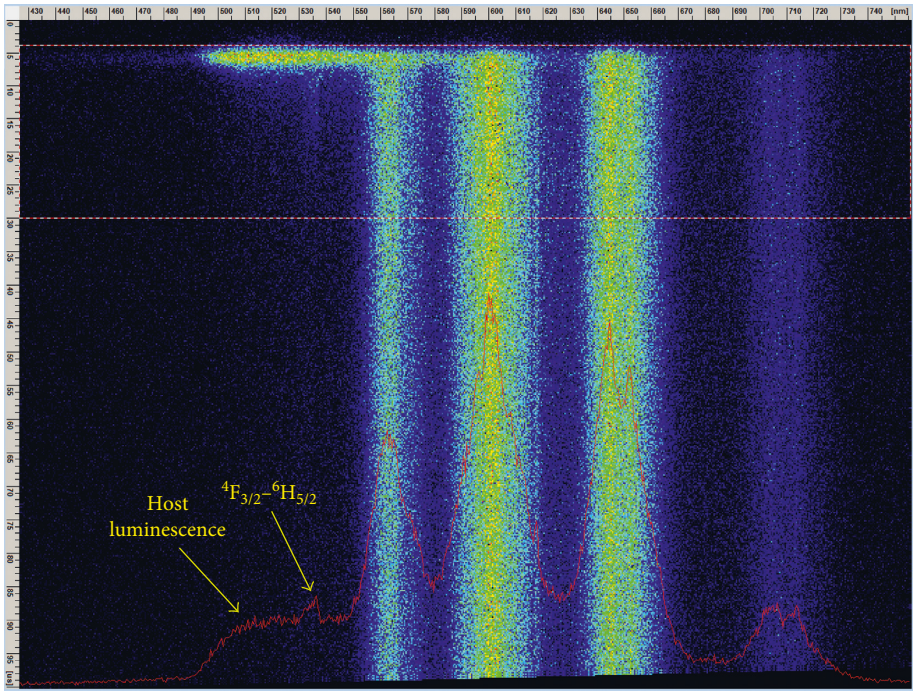

FIGURE 6: The streak image of the $GdVO_4$:Sm nanopowder. The time scale of 100 μs was adjusted for analysis of rise time of samarium lines and detection of fast host luminescence emission (OPO excitation at 330 nm).

improved by introducing the temporal dependence in the intensity ratio measurements, as proposed in [18]. Namely, it is possible to increase the sensitivity of the curve of intensity ratio between the host and samarium luminescence if an appropriately selected part of temporal evolution is used in calculation. We used the streak camera to prove the concept. The real application of this method will be based on using the gated CCD cameras and appropriate bandwidth filters for selecting the emission region of interest.

The luminescence spectra of the $GdVO_4$:Sm nanopowder were measured at various temperatures, using the OPO excitation at 330 nm and the streak camera. For calculation of intensity ratio, the narrow bands (5 nm) of host luminescence around 520 nm and the samarium line at 602 nm were used and integrated in time from their beginning. However, we varied gating times for end of signal integration. In order to apply the intensity ratio method in thermometry, it is required to fit a calibration function of analyzed thermophosphor. Based on considerations in [34, 35], we decided to use the simple empirical equation for fitting the calculated intensity ratios of experimental data: $\mathrm{IR}(T) = A + C \cdot e^{-T/\alpha}$ [34, 35], where T is the temperature in K and empirical A, C, and α are the constants obtained through fitting of measured data. The results are shown in Figure 7.

It could be seen in Figure 7 that the intensity ratio between the host luminescence band centered at 520 nm and the line at 602 nm increases with decreasing the gate time of the signal. However, decreasing the gate time decreases the integrated signal intensity, so we did not use delays smaller than 30 μs.

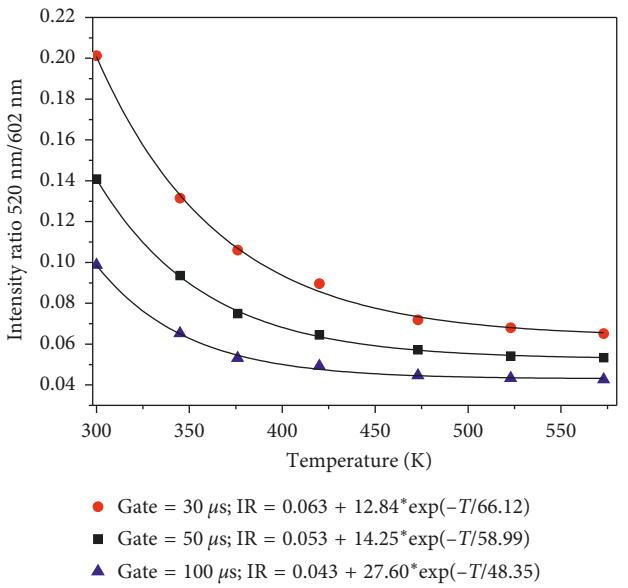

FIGURE 7: The temperature sensing calibration curve of the $GdVO_4$:Sm^{3+} nanopowder sample.

The absolute thermal sensitivity, S_a, of the intensity ratio method is defined as the rate at which IR changes with the temperature:

$$S_a = \left|\frac{d\mathrm{IR}}{dT}\right|. \quad (2)$$

The relative thermal sensitivity, S_r, of the intensity ratio method Sr is determined using the following formula:

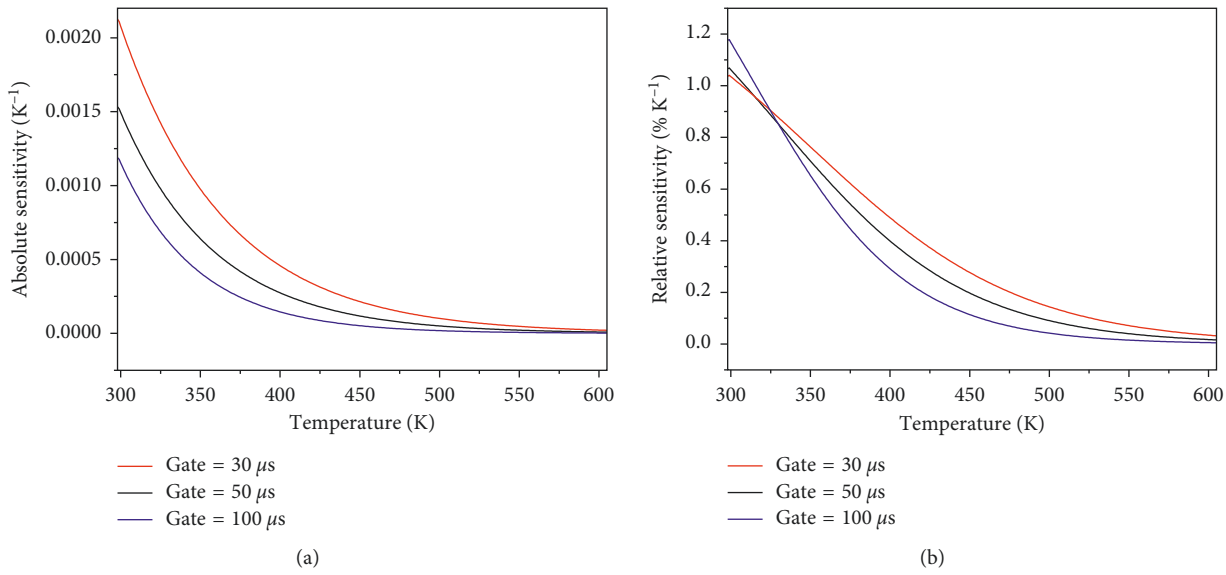

Figure 8: (a) Absolute sensitivity and (b) relative sensitivity of $GdVO_4:Sm^{3+}$ nanophosphor as a function of temperature.

$$S_r = \left|\frac{1}{\mathrm{IR}}\frac{d\mathrm{IR}}{dT}\right|. \quad (3)$$

Absolute and relative temperature sensitivities of $GdVO_4:Sm^{3+}$ nanophosphor are shown in Figure 8. The best sensitivity is obtained by the gate time of 30 μs. We estimate that this kind of temperature sensing is useful up to 500 K, where the calculated intensity ratio values stop increasing and the curve flattens, resulting in small sensitivity, even for the optimal gate time of 30 μs (see Figures 7 and 8). The proposed method provides better sensitivity than that reported in [4] for the same nanophosphor.

The CIE (Commission Internationale de l'Eclairage, 1931) chromaticity coordinates of $GdVO_4:Sm^{3+}$ are presented in Figure 9. It could be seen that the $GdVO_4:Sm^{3+}$ sample shows the orange-reddish luminescence color, and the chromaticity coordinates at room temperature are $x = 0.5963$ and $y = 0.3989$. Denoted points correspond to the temperature range from 300 K up to 673 K. The CIE diagram shows that the luminescence intensities corresponding to the last two points, 623 K and 673 K (350°C and 400°C), are obviously measured with high uncertainty, and they were not included in fitting the temperature sensing calibration curves of $GdVO_4:Sm^{3+}$.

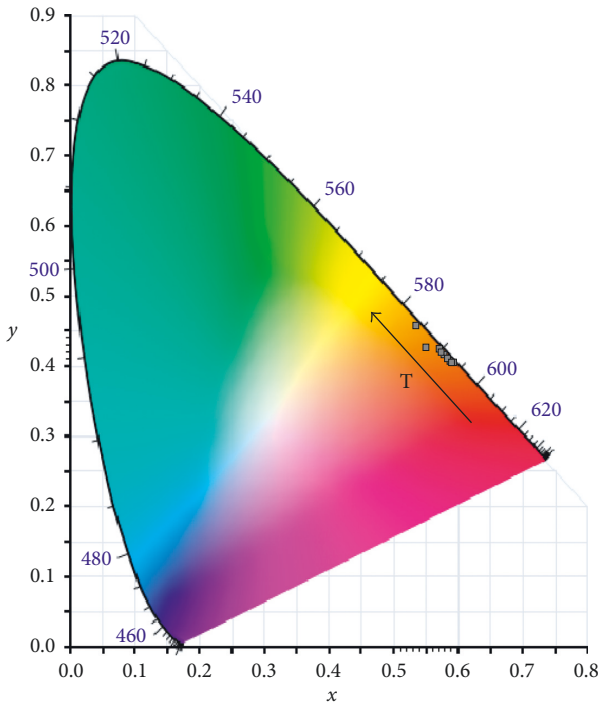

Figure 9: The CIE chromaticity diagram of emission spectra of 1 mol% $GdVO_4:Sm^{3+}$. Denoted points correspond to the temperature range from 300 K up to 673 K.

4. Conclusion

The time-resolved analysis of $GdVO_4:Sm^{3+}$ nanophosphor luminescence was conducted. The estimated lifetime of the most prominent optical emission of samarium from the $^4G_{5/2}$ level is 0.726 ms. The host luminescence was also identified. Lifetime of host luminescence is 2.82 μs. The rise time of samarium luminescence is estimated as negligible for effects that are here of interest.

We have shown that, for the analyzed $GdVO_4:Sm^{3+}$ material, the temperature sensing based on ratio of intensities of the host luminescence and the samarium line is useful up to 500 K. The used method was improved by introducing the temporal dependence in the ratio measurements. Our analysis shows that the gating time of 30 μs is optimal for acquiring the integrated luminescence intensity.

By using the CIE chromaticity diagram of emission spectra, it has been shown that this GdVO4:Sm^{3+} nanophosphor material (chromaticity coordinates $x = 0.596$, $y = 0.398$) can be used for development of orange-reddish light emitting

optical devices. We also plotted the temperature dependency of CIE chromaticity coordinates for this nanophosphor.

In summary, results of all our analyses prove that the Sm^{3+}-doped $GdVO_4$ nanopowder prepared by a simple and low-cost solution combustion synthesis method is an appropriate material for light-emitting optoelectronic devices and remote temperature sensing.

Conflicts of Interest

The authors declare that they have no conflicts of interest.

Acknowledgments

This work was financially supported within the projects of Ministry of Education, Science and Technological Development of the Republic of Serbia (OI171020).

References

[1] M. Anitha, P. Ramakrishnan, A. Chatterjee, G. Alexander, and H. Singh, "Spectral properties and emission efficiencies of $GdVO_4$ phosphors," *Applied Physics A: Materials Science & Processing*, vol. 74, no. 2, pp. 153–162, 2012.

[2] Z. Hou, P. Yang, C. Li et al., "Preparation and Luminescence Properties of YVO_4:Ln and Y(V, P)O_4:Ln (Ln = Eu^{3+}, Sm^{3+}, Dy^{3+}) nanofibers and microbelts by sol-gel/electrospinning process," *Chemistry of Materials*, vol. 20, no. 21, pp. 6686–6696, 2008.

[3] D. J. Jovanovic, Z. Antic, R. M. Krsmanovic et al., "Annealing effects on the microstructure and photoluminescence of Eu^{3+}-doped $GdVO_4$ powders," *Optical Materials*, vol. 35, no. 10, pp. 1797–1804, 2013.

[4] M. G. Nikolic, D. J. Jovanovic, V. Đorđevic, Z. Antic, R. M. Krsmanovic, and M. D. Dramicanin, "Thermographic properties of Sm^{3+}-doped $GdVO_4$ phosphor," *Physica Scripta*, vol. T149, p. 014063, 2012.

[5] S. Kaowphong, N. Chumha, P. Nimmanpipug, and S. Kittiwachana, "Nanosized $GdVO_4$ powders synthesized by sol–gel method using different carboxylic acids," *Rare Metals*, 2016.

[6] X. Li, M. Yu, Z. Hou et al., "One-dimensional $GdVO_4$:Ln^{3+} (Ln = Eu, Dy, Sm) nanofibers: electrospinning preparation and luminescence properties," *Journal of Solid State Chemistry*, vol. 184, no. 1, pp. 141–148, 2011.

[7] H. Xin, L. X. Lin, J. H. Wu, and B. Yan, "Hydrothermal synthesis and multi-color photoluminescence of $GdVO_4$: Ln^{3+} (Ln = Sm, Dy, Er) sub-micrometer phosphors," *Journal of Materials Science: Materials in Electronics*, vol. 22, no. 9, pp. 1330–1134, 2011.

[8] F. Zheng, W. Wang, and P. Yang, "$GdVO_4$: Ln^{3+} (Ln = Sm, Dy, and Er) microstructures: solvothermal and luminescent properties," *Optoelectronics and Advanced Materials: Rapid Communications*, vol. 5, no. 6, pp. 596–599, 2011.

[9] Y. Liu, G. Liu, J. Wang, X. Dong, and W. Yu, "Reddish-orange-emitting and paramagnetic properties of $GdVO_4$: Sm^{3+}/Eu^{3+} multifunctional nanomaterials," *New Journal of Chemistry*, vol. 39, no. 11, pp. 8282–8290, 2015.

[10] Y. K. Voron'ko, A. A. Sobol', V. E. Shukshin, A. I. Zagumennyĭ, Y. D. Zavartsev, and S. A. Kutovoĭ, "Raman spectroscopic study of structural disordering in YVO_4, $GdVO_4$, and $CaWO_4$ crystals," *Physics of the Solid State*, vol. 51, no. 9, pp. 1886–1893, 2009.

[11] A. A. Kaminskii, O. Lux, H. Ghee et al., "Low-temperature stimulated Raman scattering spectroscopy of tetragonal $GdVO_4$ single crystals," *Physica Status Solidi B*, vol. 251, no. 5, pp. 1045–1062, 2014.

[12] M. S. Rabasovic, D. Sevic, J. Krizan et al., "Structural properties and luminescence kinetics of white nanophosphor YAG: Dy," *Optical Materials*, vol. 50, pp. 250–255, 2015.

[13] M. S. Rabasović, D. Sević, J. Krizan, M. D. Rabasović, and N. Romcević, "Annealing effects on luminescent properties of Eu^{3+} doped $Gd_2Zr_2O_7$ nanopowders," *Science of Sintering*, vol. 47, no. 3, pp. 269–272, 2015.

[14] M. G. Nikolic, Z. Antic, S. Culubrk, J. M. Nedeljkovic, and M. D. Dramicanin, "Temperature sensing with Eu^{3+} doped TiO_2 nanoparticles," *Sensors and Actuators B: Chemical*, vol. 201, pp. 46–50, 2014.

[15] M. D. Dramicanin, Z. Antic, S. Culubrk, S. P. Ahrenkiel, and J. M. Nedeljkovic, "Self-referenced luminescence thermometry with Sm^{3+} doped TiO_2 nanoparticles," *Nanotechnology*, vol. 25, no. 48, p. 485501, 2014.

[16] V. Lojpur, M. G. Nikolic, D. Jovanovic, M. Medic, Z. Antic, and M. D. Dramicanin, "Luminescence thermometry with Zn_2SiO_4:Mn^{2+} powder," *Applied Physics Letters*, vol. 103, no. 14, p. 141912, 2013.

[17] V. Lojpur, S. Ćulubrk, and M. D. Dramićanin, "Ratiometric luminescence thermometry with different combinations of emissions from Eu^{3+} doped $Gd_2Ti_2O_7$ nanoparticles," *Journal of Luminescence*, vol. 169, pp. 534–538, 2016.

[18] M. Alden, A. Omrane, M. Richter, and G. Särner, "Thermographic phosphors for thermometry: a survey of combustion applications," *Progress in Energy and Combustion Science*, vol. 37, no. 4, pp. 422–461, 2011.

[19] B. K. Grandhe, V. R. Bandi, K. Jang, S. Ramaprabhu, S.-S. Yi, and J.-H. Jeong, "Enhanced red emission from YVO_4:Eu^{3+} nano phosphors prepared by simple co-precipitation method," *Electronic Materials Letters*, vol. 7, no. 2, pp. 161–165, 2011.

[20] S. Tang, M. Huang, J. Wang, F. Yu, G. Shang, and J. Wu, "Hydrothermal synthesis and luminescence properties of $GdVO_4$:Ln^{3+} (Ln = Eu, Sm, Dy) phosphors," *Journal of Alloys and Compounds*, vol. 513, pp. 474–480, 2012.

[21] N. Shanta Singh, R. S. Ningthoujam, M. Niraj Luwang, S. Dorendrajit Singh, and R. K. Vatsa, "Luminescence, lifetime and quantum yield studies of YVO_4:Ln^{3+} (Ln^{3+} = Dy^{3+}, Eu^{3+}) nanoparticles: concentration and annealing effects," *Chemical Physics Letters*, vol. 480, no. 4–6, pp. 237–242, 2009.

[22] G. Z. Li, Z. L. Wang, M. Yu, Z. W. Quan, and J. Lin, "Fabrication and optical properties of core–shell structured spherical SiO_2@$GdVO_4$:Eu^{3+} phosphors via sol–gel process," *Journal of Solid State Chemistry*, vol. 179, no. 8, pp. 2698–2706, 2006.

[23] H. Wang, M. Yu, C. K. Lin, and J. Lin, "Core–shell structured SiO_2@YVO_4:Dy^{3+}/Sm^{3+} phosphor particles: Sol–gel preparation and characterization," *Journal of Colloid and Interface Science*, vol. 300, no. 1, pp. 176–182, 2006.

[24] M. Yu, J. Lin, and J. Fang, "Silica spheres coated with YVO_4: Eu^{3+} layers via sol–gel process: a simple method to obtain spherical core–shell phosphors," *Chemistry of Materials*, vol. 17, no. 7, pp. 1783–1791, 2005.

[25] X. He, L. Zhang, G. Chen, and Y. Hang, "Crystal growth and spectral properties of Sm:$GdVO_4$," *Journal of Alloys and Compounds*, vol. 467, no. 1-2, pp. 366–369, 2009.

[26] V. Sudarsan, F. C. J. M. van Veggel, R. A. Herring, and M. Raudsepp, "Surface Eu^{3+} ions are different than "bulk" Eu^{3+}

ions in crystalline doped LaF_3 nanoparticles," *Journal of Materials Chemistry*, vol. 15, no. 13, pp. 1332–1342, 2005.

[27] G. Jia, Y. Song, M. Yang, Y. Huang, L. Zhang, and H. You, "Uniform YVO_4:Ln^{3+} (Ln = Eu, Dy, and Sm) nanocrystals: solvothermal synthesis and luminescence properties," *Optical Materials*, vol. 31, no. 6, pp. 1032–1037, 2009.

[28] J. Leppert, S. Peudenier, E. Bayer, B. C. Grabmaier, and G. Blasse, "Time resolved emission spectroscopy of gadolinium vanadate ceramics ($GdVO_4$:Bi^{3+})," *Applied Physics A Solids and Surfaces*, vol. 59, no. 1, pp. 69–72, 1994.

[29] F. He, P. P. Yang, N. Niu et al., "Hydrothermal synthesis and luminescent properties of YVO_4:Ln^{3+} (Ln = Eu, Dy, and Sm) microspheres," *Journal of Colloid and Interface Science*, vol. 343, no. 1, pp. 71–78, 2010.

[30] Y. Tian, B. Chen, B. Tian et al., "Size-dependent energy transfer and spontaneous radiative transition properties of Dy^{3+} ions in the $GdVO_4$ phosphors," *Journal of Nanoparticle Research*, vol. 15, no. 6, pp. 1757–1767, 2013.

[31] B. N. Tian, B. J. Chen, Y. Tian et al., "Concentration and temperature quenching mechanisms of Dy^{3+} luminescence in $BaGd_2ZnO_5$ phosphors," *Journal of Physics and Chemistry of Solids*, vol. 73, no. 11, pp. 1314–1319, 2012.

[32] H. Zhong, X. P. Li, R. S. Shen et al., "Spectral and thermal properties of Dy^{3+}-doped $NaGdTiO_4$ phosphors," *Journal of Alloys and Compounds*, vol. 517, pp. 170–175, 2012.

[33] W. P. Zhang, P. B. Xie, C. K. Duan et al., "Preparation and size effect on concentration quenching of nanocrystalline Y_2SiO_5: Eu," *Chemical Physics Letters*, vol. 292, no. 1-2, pp. 133–136, 1998.

[34] M. D. Rabasovic, B. D. Muric, V. Celebonovic, M. Mitric, B. M. Jelenkovic, and M. G. Nikolic, "Luminescence thermometry via the two-dopant intensity ratio of Y_2O_3:Er^{3+}, Eu^{3+}," *Journal of Physics D: Applied Physics*, vol. 49, no. 48, p. 485104, 2016.

[35] D. Ananias, C. D. S. Brites, L. D. Carlos, and J. Rocha, "Cryogenic nanothermometer based on the MIL-103 (Tb, Eu) metal–organic framework," *European Journal of Inorganic Chemistry*, vol. 2016, no. 13-14, pp. 1967–1971, 2016.